Annular Modes in the Extratropical Circulation. Part I: Month-to-Month Variability*

DAVID W. J. THOMPSON AND JOHN M. WALLACE

Department of Atmospheric Sciences, University of Washington, Seattle, Washington

(Manuscript received 19 October 1998, in final form 23 February 1999)

ABSTRACT

The leading modes of variability of the extratropical circulation in both hemispheres are characterized by deep, zonally symmetric or ''annular'' structures, with geopotential height perturbations of opposing signs in the polar cap region and in the surrounding zonal ring centered near 45° latitude. The structure and dynamics of the Southern Hemisphere (SH) annular mode have been extensively documented, whereas the existence of a Northern Hemisphere (NH) mode, herein referred to as the Arctic Oscillation (AO), has only recently been recognized. Like the SH mode, the AO can be defined as the leading empirical orthogonal function of the sea level pressure field or of the zonally symmetric geopotential height or zonal wind fields. In this paper the structure and seasonality of the NH and SH modes are compared based on data from the National Centers for Environmental Prediction–National Center for Atmospheric Research reanalysis and supplementary datasets.

The structures of the NH and SH annular modes are shown to be remarkably similar, not only in the zonally averaged geopotential height and zonal wind fields, but in the mean meridional circulations as well. Both exist year-round in the troposphere, but they amplify with height upward into the stratosphere during those seasons in which the strength of the zonal flow is conducive to strong planetary wave–mean flow interaction: midwinter in the NH and late spring in the SH. During these ''active seasons,'' the annular modes modulate the strength of the Lagrangian mean circulation in the lower stratosphere, total column ozone and tropopause height over mid- and high latitudes, and the strength of the trade winds of their respective hemispheres. The NH mode also contains an embedded planetary wave signature with expressions in surface air temperature, precipitation, total column ozone, and tropopause height. It is argued that the horizontal temperature advection by the perturbed zonal-mean zonal wind field in the lower troposphere is instrumental in forcing this pattern.

A companion paper documents the striking resemblance between the structure of the annular modes and observed climate trends over the past few decades.

1. Introduction

Month-to-month and winter-to-winter fluctuations of the Northern Hemisphere (NH) lower-stratospheric wintertime polar vortex are strongly coupled with a wave-like pattern of geopotential height anomalies in the middle troposphere that resembles the North Atlantic Oscillation (NAO; Baldwin et al. 1994; Perlwitz and Graf 1995; Cheng and Dunkerton 1995; Kitoh et al. 1996; Kodera et al. 1996). Thompson and Wallace 1998 (hereafter TW98) showed that the surface signature of this coupled pattern corresponds to the leading empirical orthogonal function (EOF) of NH wintertime monthly mean sea level pressure (SLP), which, like the variations at stratospheric levels, is dominated by a zonally symmetric, meridional seesaw in atmospheric mass between the Arctic and the midlatitudes (Kutzbach 1970; Trenberth and Paolino 1981; Wallace and Gutzler 1981). To distinguish the leading EOF of the NH SLP field from the somewhat more regional pattern derived from monthly indices of the NAO, they referred to it as the Arctic Oscillation (AO). TW98 showed that during the NH cold season (November–April), regression patterns based on an index of the AO exhibit a distinct signature in the geopotential height and temperature fields marked by 1) a zonally symmetric, equivalent barotropic structure that amplifies by a factor of ~5 from the surface to the lower stratosphere, and 2) a tropospherically confined baroclinic signature. Based on the nearly perfect correlation between time series of the geopotential height patterns at various levels, TW98 argued that the above are components of a single modal structure, in which the baroclinic features are induced by horizontal temperature advection by the zonally symmetric component of the flow acting upon the large east–west thermal contrasts at high latitudes during the NH winter.

Gong and Wang (1999) pointed out that the AO bears at least a superficial resemblance to the leading mode of low-frequency variability in the Southern Hemi-

* JISAO Contribution Number 694.

Corresponding author address: Dr. David W. J. Thompson, Joint Institute for the Study of the Atmosphere and Ocean, University of Washington, Box 354235, Seattle, WA 98195-4235.
E-mail: davet@atmos.washington.edu

TABLE 1. Datasets used in this study. Unless otherwise noted, periods of record include all of the first and last years listed.

	Period of record	Source
Surface air temperature	1900–97	CRU at University of East Anglia (Jones 1994; Parker et al. 1995)
Sea level pressure	1900–97	Data Support Section at NCAR (Trenberth and Paolino 1980)
Geopotential height	1958–97	NCEP–NCAR reanalysis via NOAA CDC (Kalnay et al. 1996)
Temperature	1958–97	NCEP–NCAR reanalysis via NOAA CDC (Kalnay et al. 1996)
Total column ozone	11/1978–4/1993	*Nimbus-7* TOMS via NASA GSFC (NASA 1978)
MSU-4 temperature	1/1979–8/1997	MSU-4 temperature via NASA MSFC (Spencer and Christy 1993)
COADS surface wind	1958–95	Data Support Section at NCAR (Woodruff et al. 1987, 1993)

sphere (SH) troposphere, which exists year-round and is characterized by an equivalent barotropic, zonally symmetric structure involving exchanges of mass between the mid- and high latitudes. This SH mode emerges as the leading EOF of zonally varying geopotential height based on station data (Szeredi and Karoly 1987), gridded analyses of SLP (Rogers and van Loon 1982; Gong and Wang 1999), 500-hPa height (Rogers and van Loon 1982; Kidson 1988b), and 300-hPa height (Karoly 1990). It has also been identified as the leading EOF of the SH zonally averaged geopotential height field at 1000 hPa (Shiotani 1990), the zonally averaged zonal wind at 500 hPa (Kidson 1988a), and in the 1000–100-hPa layer (Yoden et al. 1987; Hartmann and Lo 1998). Is the similarity between this SH mode and the AO fortuitous, or are these ''annular modes'' reflections of dynamical processes whose commonality transcends the striking contrasts between the NH and SH land–sea geometry and orography? To address this question, we will perform a side-by-side comparison of the structure and seasonality of the NH and SH annular modes based on monthly mean data. Our analysis of the SH annular mode extends the previous studies cited above by documenting its seasonally varying coupling with the stratosphere.

This paper is composed of seven sections. Section 2 describes the data sources used and the methods of analysis. Section 3 shows that, like the SH annular mode, the AO is a robust structure that emerges as the primary mode of month-to-month variability in the zonally varying lower-tropospheric geopotential height field and the zonally symmetric component of the geopotential height field from the surface to the lower stratosphere. Section 4 documents the seasonality of the annular modes. It is shown that both the NH and SH modes are evident throughout the year in the troposphere, and that during limited times of year when planetary waves are able to penetrate into the stratosphere, the annular modes amplify with height into the polar lower stratosphere. In section 5, the vertical structures of the annular modes during the stratosphere's active and inactive seasons are contrasted and shown to be remarkably similar in the NH and SH. Section 6 offers evidence suggesting that the zonally varying lower-tropospheric thermal structure associated with the AO corresponds closely to the pattern of temperature advection by the zonal-mean zonal flow in the lower troposphere, and that the SH mode has an analogous but more localized signature in surface air temperature. This section also documents the signatures of the annular modes in total column ozone. The final section offers a synthesis and partial interpretation of the results. Further interpretation is offered in the final section of Part II (Thompson et al. 2000).

2. Data and analysis techniques

The sources and periods of record of the various gridded datasets used in this study are listed in Table 1. The primary dataset is the National Centers for Environmental Prediction–National Center for Atmospheric Research (NCEP–NCAR) reanalysis (Kalnay et al. 1996) obtained from the National Oceanic and Atmospheric Administration (NOAA) Climate Diagnostics Center (CDC). The data are gridded on a 2.5°lat $\times$ 2.5° long mesh. Because of concerns about possible discontinuities in the SLP field derived from the NCEP–NCAR reanalysis, we use SLP provided courtesy of the Data Support Section at NCAR (Trenberth and Paolino 1980). In the lower stratosphere we supplement the NCEP–NCAR reanalysis with total column ozone derived from the *Nimbus-7* Total Ozone Mapping Spectrometer (TOMS version 7) from the National Aeronautics and Space Administration (NASA) Goddard Space Flight Center (GSFC) and lower-stratospheric temperature data derived from the Microwave Sounding Unit Channel 4 (MSU-4) from the NASA Marshall Space Flight Center (MSFC; Spencer and Christy 1993).

We make extensive use of principal component analysis (PCA) of the temporal (unstandardized) covariance matrix to determine the primary modes of month-to-month variability in various fields. In all cases, monthly mean gridded data are weighted by the square root of cosine of latitude to ensure that equal areas are afforded equal weight in the analysis. In a similar manner, when the analysis is applied to more than a single height level, the data are weighted by the square root of the pressure interval represented by that level (i.e., by their mass-weighted contribution to the variance). Rather than displaying the actual EOFs with their inherent weighting functions, we regress the monthly mean unweighted anomaly fields upon the standardized leading principal component (PC) time series and display the resulting covariances or regression coefficients. Because the standardized PC time series are dimensionless, these ''regression maps'' have the same units as the anomaly field itself. The amplitudes shown in the regression maps therefore correspond to anomaly values in that field that occur in association with a one standard deviation anomaly in the index time series and can thus be considered typical amplitudes. Note that the regression maps are not, strictly speaking, EOFs because of the cosine weighting (and density weighting when using more than one geopotential height level) that is applied.

The lower-tropospheric geopotential height field plays an important role in our analysis. As noted above, results for the NH are based on SLP. In order to facilitate comparison with geopotential height fields aloft, we express the results in terms of the equivalent anomalies in 1000-hPa geopotential height using the approximate relationship $Z_{1000} = 8(\mathrm{SLP} - 1000\ \mathrm{hPa})$ where Z_{1000} is the height of the 1000-hPa surface. In the SH, we use 850-hPa geopotential height Z_{850} rather than SLP to partially alleviate the ambiguities introduced by the reduction to sea level over the high terrain of Antarctica.

3. The annular modes in the geopotential height field

This section presents evidence that the leading mode of month-to-month variability in the geopotential height field is fundamentally zonally symmetric not only in the SH, but also in the NH. As evidence we show that a time series very similar to the leading PC of the zonally varying SLP field can be recovered from PCA of the zonally averaged geopotential height field. The analyses in this section are based upon monthly mean data for all calendar months from 1958 through 1997.

The structure of NH (poleward of 20°N) SLP anomalies regressed upon their leading PC time series (Fig. 1d) is virtually identical to that derived from the analysis of TW98, which was restricted to the months of November–April. It also closely resembles the results of Kutzbach (1970), Trenberth and Paolino (1981), and Wallace and Gutzler (1981). The spatial structure of SH (poleward of 20°S) 850-hPa geopotential height anomalies regressed upon their leading PC time series (Fig. 1c) is reminiscent of the leading EOF of the SH SLP field (Rogers and van Loon 1982), 500-hPa height field (Rogers and van Loon 1982; Kidson 1988b), and 300-hPa height field (Karoly 1990). As documented in Table 2, both of these modes account for substantial fractions of the total month-to-month variance of their respective fields and are well separated from the other PCs as per the criterion of North et al. (1982).

The NH and SH structures shown in the bottom panels of Fig. 1 are predominantly zonally symmetric (the SH structure somewhat more so) and are characterized by north–south seesaws of atmospheric mass between the high latitudes and parts of the midlatitudes. The two modes exhibit similar amplitudes and meridional scales. The corresponding standardized PC time series will respectively be referred as the indices of the annular modes, that is, the AO and its SH counterpart.

The vertical structures of the zonally symmetric zonal wind anomalies observed in association with the annular modes, shown in the top panels of Fig. 1, are very similar. The SH structure is consistent with results of Yoden et al. (1987), Kidson (1988b), Karoly (1990), and Hartmann and Lo (1998). In both hemispheres, the annular modes are dominated by meridional dipoles with nodes centered ~45°. The high-latitude centers of action have maxima centered near 57.5° in the lower troposphere, tilting poleward with height to ~65° in the upper troposphere–lower stratosphere. The poleward wind maximum of the AO amplifies with height upward into the lower stratosphere, whereas the strongest wind anomalies in the SH annular mode are observed in the upper troposphere. We will show in the next section that upward amplification into the stratosphere is in fact observed in both modes, but only in certain seasons.

The zonal symmetry of the leading EOFs of SLP (Fig. 1) suggests that these modes make important contributions to the variance of the zonally averaged geopotential height field. Their signatures are, in fact, reflected in the meridional profiles of the month-to-month variance of zonally averaged SLP and 1000-hPa geostrophic wind (Fig. 2). The variance of monthly mean, zonal-mean SLP does not increase monotonically with latitude (as might be expected in the absence of a zonally symmetric mode of variability): the variance profile exhibits well-defined shoulders near 45° lat in both hemispheres (Fig. 2a). Consistent with this feature, the variance of the zonal-mean zonal wind field at 1000 hPa exhibits distinct maxima ~25°–35° and ~55°–60° latitude in both hemispheres (Fig. 2b). These features are particularly impressive in the NH during the winter season of November–April (dashed lines).

The characteristic features of the zonally symmetric circulation revealed in Fig. 2 emerge as the leading mode of variability in the zonal-mean circulation from the surface upward into the lower stratosphere. Figure 3 shows lower-tropospheric geopotential height and zonally averaged zonal wind regressed onto the leading standardized PC time series of the monthly mean, zon-

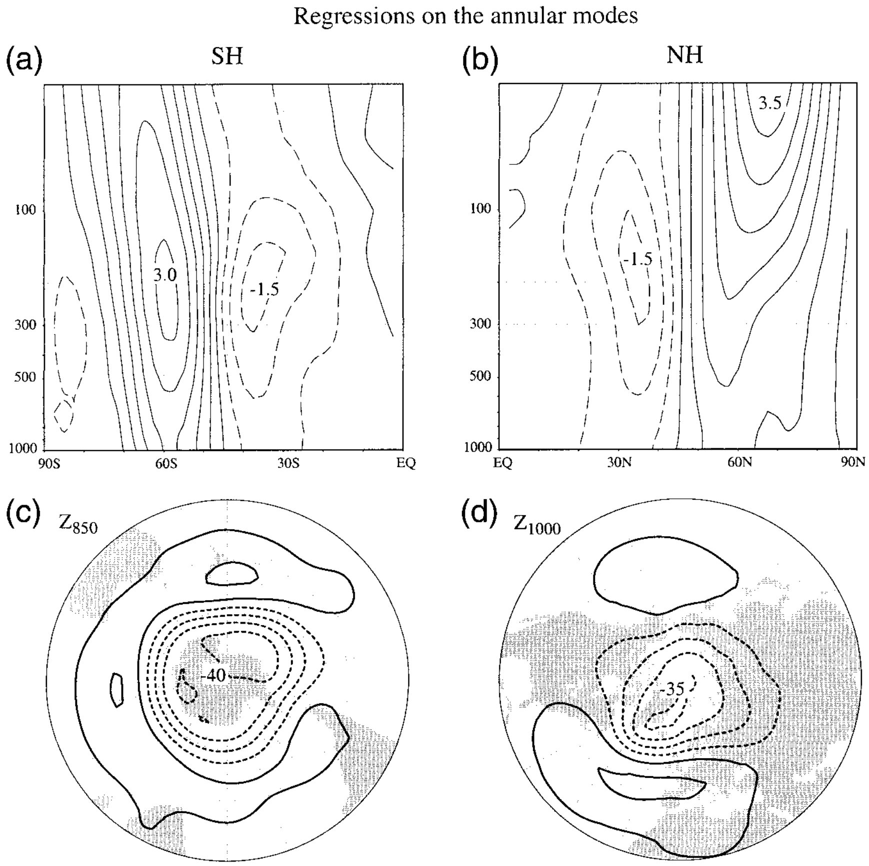

FIG. 1. (top) Zonal-mean geostrophic wind and (bottom) lower-tropospheric geopotential height regressed on the standardized indices of the annular modes (the AO and its SH counterpart) based upon monthly data, Jan 1958–Dec 1997. Left panels are for the SH, right panels are for the NH. Units are m s^{-1} (top) and m per std dev of the respective index time series (bottom). Contour intervals are 10 m (−15, −5, 5, . . .) for geopotential height and 0.5 m s^{-1} (−0.75, −0.25, 0.25) for zonal wind.

ally averaged geopotential height field from 20° to 90° and 1000 to 50 hPa in both hemispheres. Both PCs explain large fractions of the variance (45% in the NH, 47% in the SH; see Table 2). The similarity between these structures and the corresponding patterns derived from the leading PCs of the zonally varying lower-tropospheric geopotential height field (Fig. 1) is striking. In fact, the PC time series used to construct Figs. 1 and 3 are correlated with one another at a level of 0.85 in the NH and 0.95 in the SH. Similar structures emerge in regression patterns based on the leading PCs of zonal-mean zonal wind in each hemisphere (again from 20° to 90° and 1000 to 50 hPa). In those patterns (not shown) the equatorward center of action in the zonal wind field is slightly more prominent: the leading PC time series of the zonal-mean zonal wind and the geopotential height fields are correlated with one another at a level of 0.81 in the NH and 0.91 in the SH.

TABLE 2. Percentage of variance explained by the leading modes in EOF expansion of monthly mean fields for the region poleward of 20°, based on data for all calendar months: mode 1 (2, 3).

	Zonally varying SLP (NH) and Z_{850} (SH)	Zonal-mean geopotential height (1000 to 50 hPa)	Zonal-mean zonal wind (1000 to 50 hPa)
NH	20 (10, 10)	45 (17, 12)	35 (24, 12)
SH	27 (12, 9)	47 (27, 10)	45 (22, 9)

4. Seasonality

To document the seasonally varying climatology of the annular modes we use a series of scatterplots (Fig. 4) constructed from daily mean NCEP–NCAR reanalysis data in the following manner: 1) the annual march (based on 40 yr of monthly data interpolated to daily resolution) was removed from the time series at each grid point; 2) anomalies were averaged over the polar cap region (65°–90° N/S in the lower troposphere; 70°–90° N/S in the lower stratosphere) for each day from 1 January 1958 to 31 December 1997; 3) the time series for all 40 yr were plotted together as a function of day of calendar date.

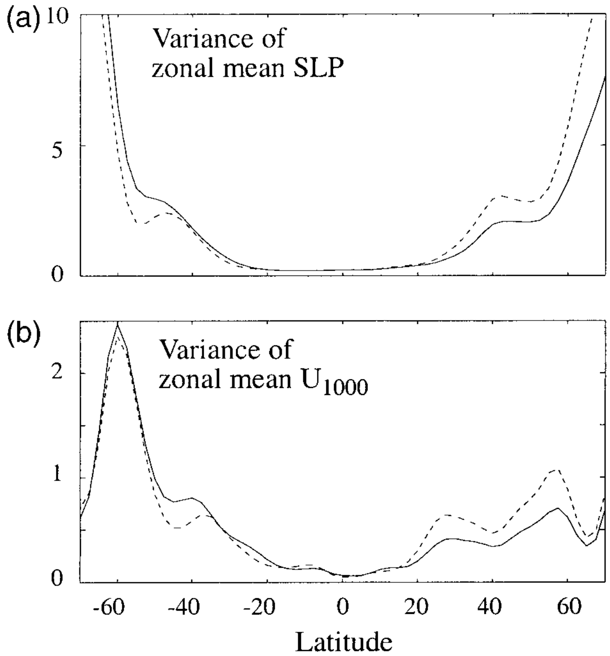

FIG. 2. (a) Variance of zonal-mean SLP and (b) zonal-mean zonal wind at 1000 hPa calculated from monthly mean anomalies for all months of the year (solid line) and Nov–Apr (dashed line). Vertical tickmarks are at intervals of 5 hPa^2 for SLP and 0.5 $m^2\ s^{-2}$ for 1000-hPa zonal wind.

The bottom two panels in Fig. 4 show these daily anomalies for the 1000-hPa height field (NH) and the 850-hPa height field (SH). In both hemispheres there is an annual march in the variance, with higher amplitudes during the cold-season months (November–April in the NH and May–October in the SH). The annual march is more pronounced in the NH owing to the lower variance during the warm season. Figure 5 shows the structure of the NH 1000-hPz and SH 850-hPa monthly mean anomaly height fields regressed upon the leading PCs computed separately for these contrasting seasons. In all cases the leading mode is unique with respect to the other eigenmodes (Table 3). In the SH, the spatial structures for the warm and cold seasons are both nearly zonally symmetric, with similar amplitude and similar meridional scale, and they resemble the leading mode of variability based on all calendar months shown in Figs. 1 and 3. The leading NH mode also exhibits a high degree of zonal symmetry during both seasons, but its amplitude and meridional scale are somewhat larger during the cold season. Hence, the structure shown in Fig. 1d is largely dominated by the NH cold season. Despite its smaller meridional scale, the NH warm-season PC time series is correlated with the PC time series based on all calendar months at a level of 0.97.

The middle panels in Fig. 4 show daily 50-hPa height anomalies averaged over the polar cap regions (hereafter denoted $\langle Z_{50} \rangle$), which exhibit much more distinct "active" and "inactive" seasons in both hemispheres. In the NH the variability is largest during January–March (JFM), whereas in the SH it is largest in springtime from mid-October to mid-December. The NH inactive season is quieter than its SH counterpart. In both hemispheres, the frequency distribution of $\langle Z_{50} \rangle$ is slightly skewed: positively during most of the active season when episodic warmings are responsible for most of the variability, but negatively toward the end of the active season, when much of the variability is a consequence of delays in the final breakdown of the polar vortex.

While the active season in the NH stratosphere coincides with the cold season at the surface, it is delayed by several months in the SH. To explore the reasons for this delay, and for the apparent skewness, we show in the top panel of Fig. 4 daily values of $\langle Z_{50} \rangle$, including the climatological mean annual march. Because 50-hPa height in the Tropics never departs much from its annual-mean value, indicated by the horizontal line, the points in these plots are also indicative of the meridional gradient in the 50-hPa height field in the respective hemispheres: points below the line are indicative of an equator–pole gradient consistent with westerly flow, and vice versa. In the NH, the variance of $\langle Z_{50} \rangle$ is largest when the westerly polar vortex is strongest, whereas in the SH it is largest at the time when the vortex is in the process of breaking down. When the vortex is easterly there is relatively little variance in $\langle Z_{50} \rangle$. The SH polar cap is also quiescent during midwinter when the vortex attains a strength far in excess of its NH counterpart. In both hemispheres, the active season thus corresponds to months in which the flow is westerly in the lower stratosphere, but less than some threshold value. If fluctuations in $\langle Z_{50} \rangle$ are a manifestation of planetary wave–mean flow interaction, the observed seasonality is, for the most part, consistent with the predictions of Charney and Drazin (1961). One notable discrepancy is the absence of a SH maximum during April–May when the vortex is building up. In fact, radiosonde temperature measurements presented in Randel and Wu (1999) suggest the existence of a peak at that time.

Based on the results presented in the top panels of Fig. 4, we define two kinds of inactive seasons in the SH lower stratosphere: one when the vortex is strong westerly, and the other when the vortex is weak or easterly. The seasons chosen for further analysis of the relationship between the stratosphere and troposphere are as follows:

1) Active seasons: SH: November (N), NH: January–March (JFM);
2) Inactive season, strong westerly vortex: SH: June–August (JJA), NH: none;
3) Inactive season, weak or easterly vortex: SH: February–March (FM), NH: JJA.

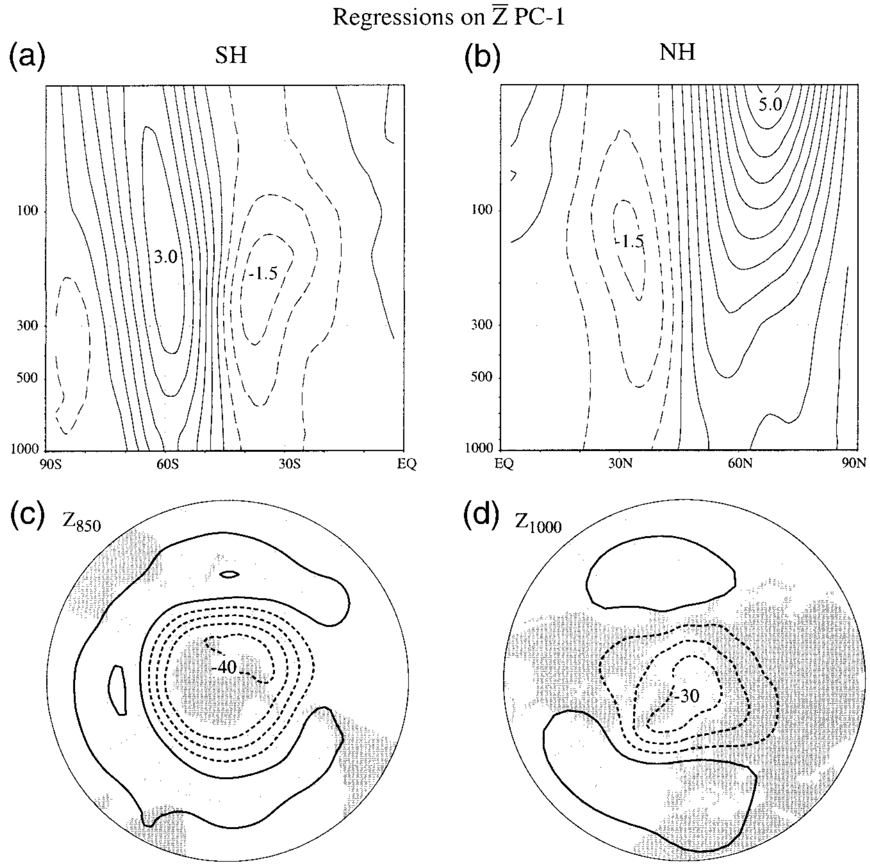

FIG. 3. As in Fig. 1, but regression maps are based on the standardized leading PC time series of the zonal-mean geopotential height field (1000–50 hPa; 20°–90°).

Transitional months such as October and December in the SH are omitted in order to ensure at least one month's separation between seasons. These so-defined active and inactive seasons are the framework for the analysis in the next two sections.

Whereas the annular modes are present year-round in the lower-tropospheric height field (Tables 3 and 4), it is only during the stratosphere's active season in the respective hemispheres that a distinct leading mode resembling the surface signature of the annular modes is recovered in the 50-hPa height field. The top panels in Fig. 6 show the leading mode of the 50-hPa height field for these active seasons (i.e., November in the SH and JFM in the NH). These modes explain a large fraction of the variance in their respective fields (Table 5) and are both nearly zonally symmetric, with meridional scales comparable to those in the surface signatures of the annular modes. The NH pattern resembles the leading EOF of 50-hPa height shown in Perlwitz and Graf (1995), Kitoh et al. (1996), Kodera et al. (1996), and TW98 for the NH cold-season months, and it also resembles the leading mode of coupling with the tropospheric circulation shown by Baldwin et al. (1994), Perlwitz and Graf (1995), and Cheng and Dunkerton (1995). During these active seasons the surface signatures of the annular modes can be recovered by regressing the lower-tropospheric height field onto the leading PC time series of the zonally varying 50-hPa height (Z_{50}) field in the respective hemispheres (Fig. 6, bottom panels). During the inactive summer seasons when the vortex is weak (or easterly), the meridional scale of the leading mode of 50-hPa variability (not shown) is larger and the amplitude of this mode is much weaker. During the midwinter inactive season in the SH (JJA) when the polar vortex is excessively strong, the variance exhibits largest amplitude in a ring surrounding the pole, rather than over the pole itself.

5. Structure of the annular modes during the stratosphere's active and inactive seasons

The zonal-mean vertical structure of the annular modes is now examined for the contrasting active and inactive seasons in the polar lower stratosphere, as defined in the previous section. The results are displayed as regression maps based on the indices defined in sec-

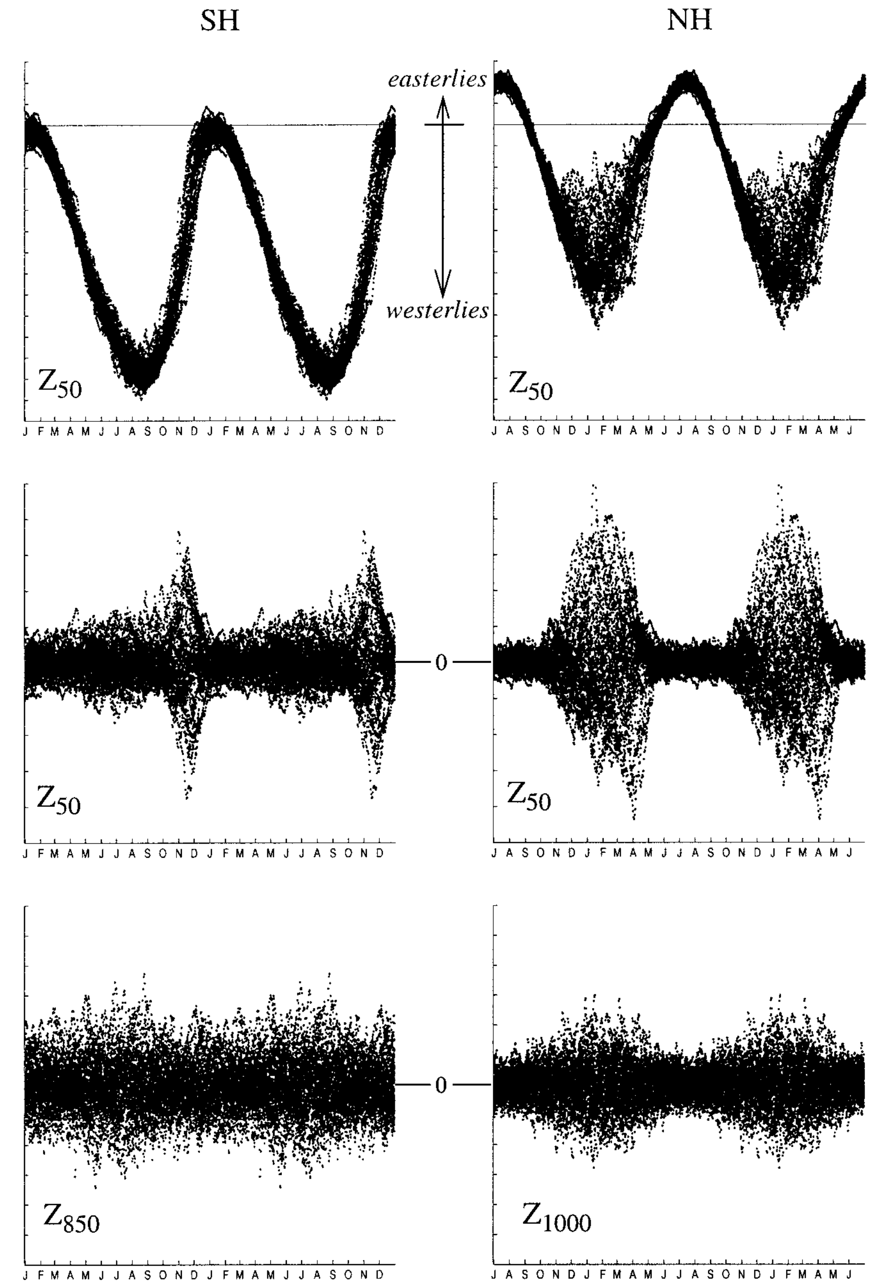

FIG. 4. (top) Daily mean 50-hPa height averaged over the region poleward of 70° for the 40-yr period 1958–97 plotted as a function of calendar day. (middle) As in the top panel but with the climatological mean removed. (bottom) As in the middle panel but for lower-tropospheric height averaged over the region poleward of 65°. Left panels are for the SH, right panels are for the NH. Calendar months (on the ordinate axis) are lagged by 6 months between hemispheres, and the annual cycle is repeated. In the top panel, the horizontal line indicates the annual-mean, tropical (20°N–20°S) 50-hPa height. Values below this line indicate an equator–pole gradient consistent with westerly flow, and vice versa. Tick marks are at intervals of 200 m for 50-hPa height and 50 m for 1000-hPa (850 hPa) height.

tion 3. The appropriate monthly segments of these year-round time series are used as a basis for defining the structure of the NH and SH annular modes for the respective seasons. It is permissible to use year-round indices because their seasonal segments are very highly correlated with the PC time series determined from seasonal subsets of the 1000-hPa (NH) and 850-hPa (SH) data (section 4).

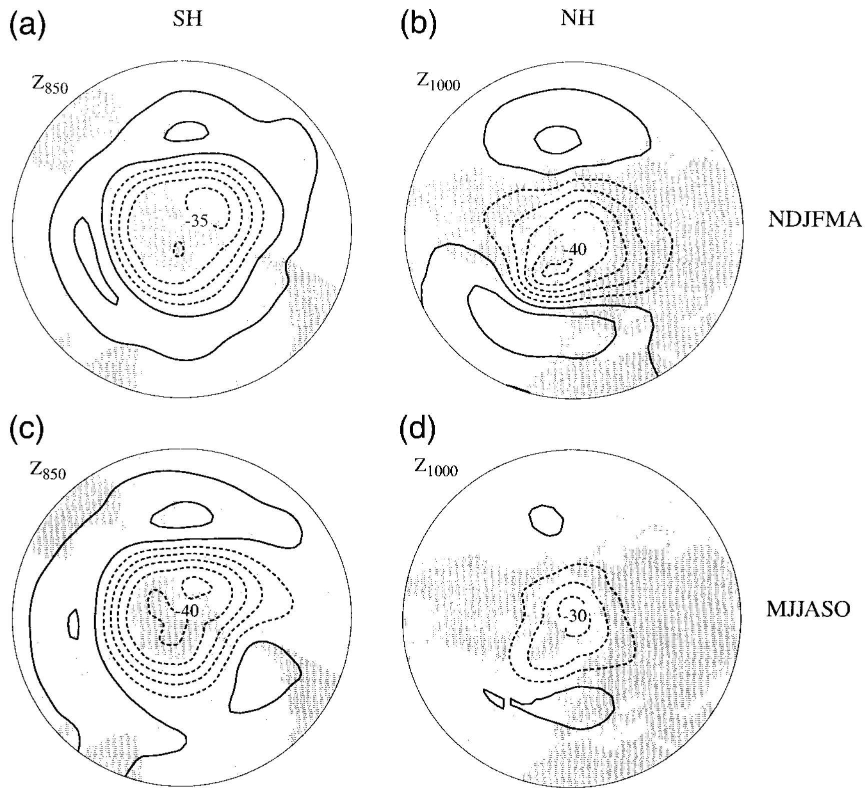

FIG. 5. Leading modal structures of the monthly mean SLP anomaly (NH) and 850-hPa height anomaly (SH) fields for (top) Nov–Apr and (bottom) May–Oct displayed as regression maps based on their standardized PC time series. Contour intervals as in Fig. 1.

a. Active seasons: SH November and NH JFM

The top panels in Fig. 7 show the zonal-mean zonal wind and mean meridional circulations regressed onto the active season segments of the indices of the NH and SH annular modes for the domains extending from equator to pole and from 1000 to 30 hPa. The vertical motion field is not provided above the 100-hPa level in the NCEP–NCAR reanalysis, and it is also not shown in the Tropics where the anomalies were found to be noisy and subject to large sampling variability. The positive (high index) polarity of the annular modes is defined as below-normal heights over the polar cap region (i.e., as displayed in Fig. 1). Since the analysis is linear, we need describe each map in terms of the positive polarity only.

The patterns of zonal-mean zonal wind anomalies associated with the NH and SH annular modes during the active seasons are remarkably similar. Both assume the form of a meridional dipole in which the wind anomalies exhibit an equivalent barotropic structure. The positive polarity is marked by easterly anomalies in the equatorward center of action and westerly anomalies in the poleward center. The easterly anomalies extend equatorward into the subtropics near the surface (particularly in the NH), whereas they exhibit a narrower maximum at ~37° at the 200-hPa level. The westerly anomalies amplify with height from the surface upward into the lower stratosphere, the axis tilting slightly poleward from ~58° in the troposphere to ~65° at the 50-hPa level.

The (zonal) mean meridional circulation anomalies associated with the NH and SH annular modes both assume the form of paired high-latitude and subtropical

TABLE 3. Percentage of variance explained by the leading modes in EOF expansion of monthly mean fields for the region poleward of 20°, for seasons indicated: mode 1 (2, 3).

	Nov–Apr	May–Oct
NH SLP	21 (12, 11)	16 (9, 8)
SH Z_{850}	28 (10, 9)	27 (15, 10)

TABLE 4. Statistics for the leading EOFs of selected monthly mean fields and seasons, as indicated.

	Spatial correlation with EOF 1 in Fig. 1	Variance explained: mode 1 (2, 3)
SH Z_{850} Feb–Mar	0.96	32 (10, 7)
SH Z_{850} Nov	0.92	26 (13, 10)
SH Z_{850} Jun–Aug	0.99	29 (13, 10)
NH SLP Jan–Mar	0.99	26 (13, 10)
NH SLP Jun–Aug	0.82	19 (8, 7)

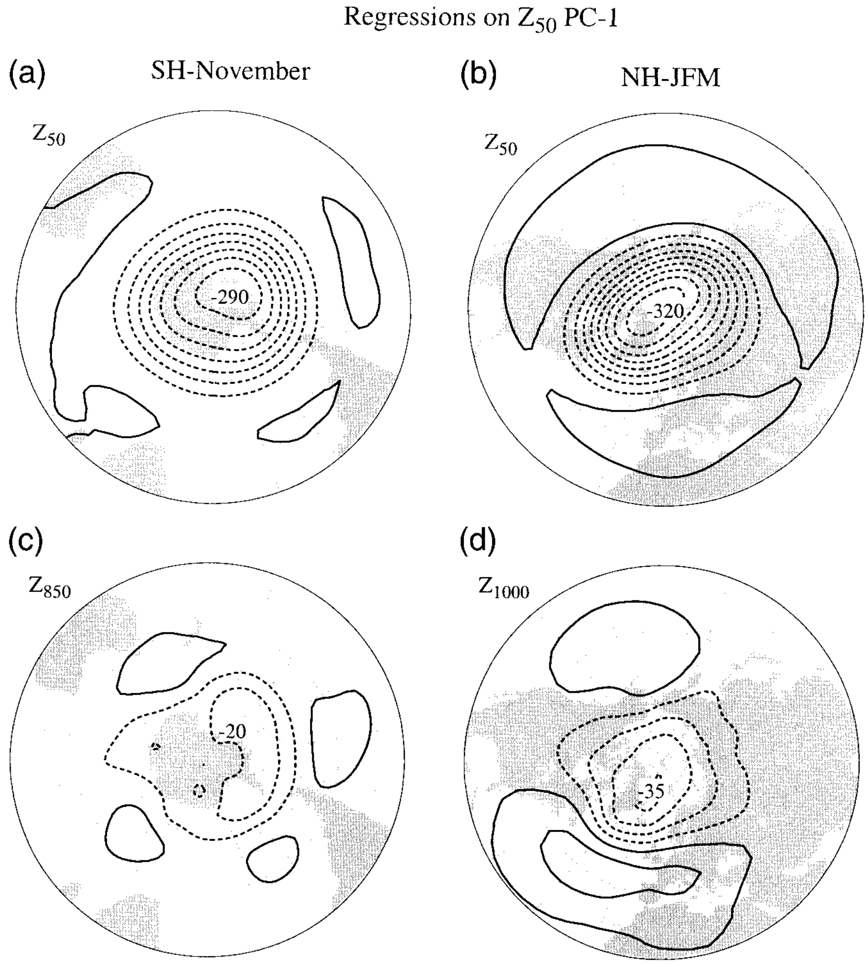

FIG. 6. (Top) Leading modal structures of the monthly mean 50-hPa height anomaly field for Nov (SH) and Jan–Mar (NH) displayed as regression maps based on their standardized PC time series. (Bottom) 1000- (NH) and 850-hPa (SH) height fields regressed onto the leading PC time series of the 50-hPa height modes depicted above. Contour intervals as in Fig. 1 for 1000- and 850-hPa height and 40 m (-60, -20, 20, . . .) for 50-hPa height.

cells. In the positive polarity, the polar cell is characterized by anomalous rising motion over subpolar latitudes and subsidence between ~40° and 50°. The weaker subtropical cell circulates in the opposite sense. The high-latitude cells extend to somewhat higher levels than the subtropical cells, and the SH cell clearly extends above the 100-hPa level. In the upper branch of the high-latitude cells, anomalous equatorward flow prevails across the axis of the maximum westerly wind anomalies. The Coriolis force acting on this flow imparts an easterly acceleration that must be balanced by anomalous eddy flux convergence. Similarly, the Coriolis force induced by the anomalous poleward flow across the axis of the upper-tropospheric easterly wind anomalies must be balanced by anomalous eddy flux divergence. Hence, as noted in Yoden et al. (1987), Shiotani (1990), Karoly (1990), Kidson and Sinclair (1995), and Hartmann and Lo (1998), the annular modes are accompanied by an anomalous poleward eddy flux of westerly momentum in the upper troposphere centered near 45° lat that maintains the zonal wind anomalies in the free atmosphere. The anomalous high-latitude cells, which are in the same sense as the climatological mean Ferrell cells, act to maintain the anomalous westerlies in the subarctic against frictional dissipation. Similarly, the anomalous surface easterlies in the subtropics appear to be maintained by the Coriolis force acting on the equatorward branch of the anomalous equatorward flow

TABLE 5. Percentage of variance explained by the leading modes in EOF expansion of monthly mean fields for the region poleward of 20°, for calendar months indicated: mode 1 (2, 3).

	Variance explained: mode 1 (2, 3)
NH Z_{50} Jan–Mar	54 (13, 8)
SH Z_{50} Nov	56 (14, 11)

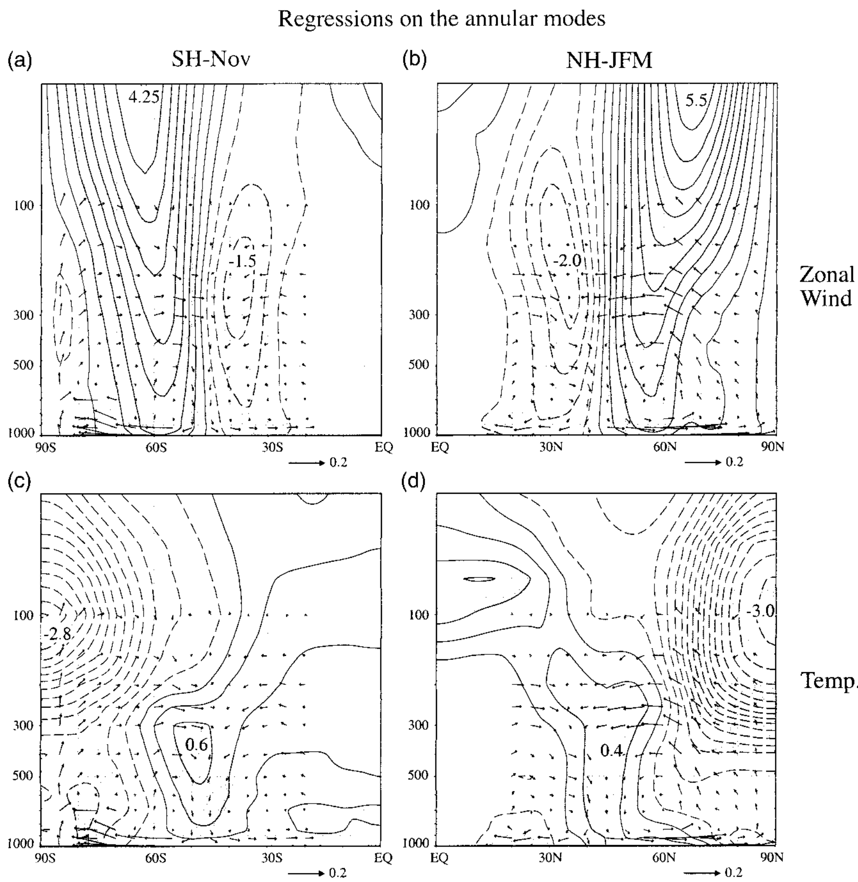

FIG. 7. (top) Zonal-mean zonal flow (contours) and mean meridional circulation (vectors) regressed onto the standardized monthly time series of the annular modes (the AO and its SH counterpart) for the active seasons Jan–Mar (NH) and Nov (SH) based on monthly data from 1958 to 1997. (bottom) As in the top panel but contours are for zonal-mean temperature. Contour intervals are 0.5 m s^{-1} (-0.75, -0.25, 0.25) for zonal wind and 0.2 K (-0.3, -0.1, 0.1) for temperature. Vectors are in units of m s^{-1} for the meridional wind component; cm s^{-1} for the vertical component (scale at bottom). Shading indicates correlations of $r > 0.4$.

in the subtropical cell, which may be regarded as an enhancement of the Hadley cell.

The bottom panels in Fig. 7 show zonal-mean temperature regressed onto the same indices. In both hemispheres, the positive polarity of the annular mode is marked by anomalously cold polar cap regions, indicative of adiabatic cooling. The lower-stratospheric ascent appears to be more pronounced in the SH. Positive temperature anomalies are observed throughout the depth of the troposphere in a band centered near 45°, coincident with the descending branch of the anomalous meridional circulation. Shallow warm anomalies are also evident near the surface in the NH between 55° and 75°N (but not in the SH). This feature is likely due to the zonally asymmetric warming of Eurasia that accompanies the positive polarity of the AO, as discussed in TW98 and in the following section of this paper. The positive temperature anomalies in the 40°–50° belt are overlain by negative anomalies in the lower stratosphere, suggestive of a lifting of the tropopause within this band of anomalous anticyclonic shear at the jet stream level. Positive temperature anomalies are also evident in a layer extending upward and equatorward from the midlatitude troposphere to the tropical tropopause.

To assess the significance of the warming at the tropopause level in the Tropics we regressed the active season zonal wind and temperature anomalies in each hemisphere onto a standardized time series of tropical (20°N–20°S) tropopause temperature anomalies, which might be viewed as representing a radically different definition of the annular modes. The resulting regression patterns (Fig. 8) are qualitatively similar to the patterns based on the extratropical indices. They illustrate more clearly the out-of-phase relationship between tropical and polar temperatures at the tropopause level, which is indicative of a modulation of the intensity of the Lagrangian mean meridional circulation by the annular modes. These results are reproducible using, as a reference time series, tropical mean (20°N–20°S) temper-

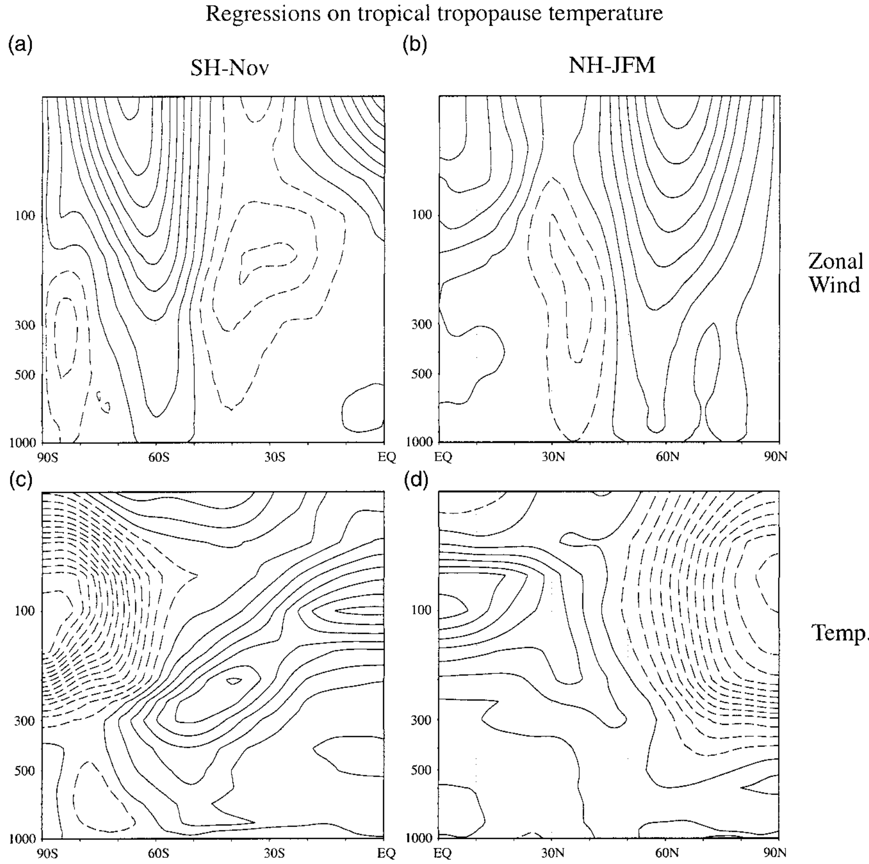

FIG. 8. (top) Zonal-mean zonal wind and (bottom) temperature regressed upon standardized tropical mean (20°N–20°S) tropopause temperature for the months of Nov (SH) and Jan–Mar (NH). Contour intervals as in Fig. 7.

ature at the 100-hPa level, and also temperature derived from the MSU-4 data (representative of the 150–50-hPa layer) for the period January 1979–August 1997 (not shown).

b. Inactive seasons: SH FM and NH JJA

The zonal wind structures for the summer inactive seasons, shown in the upper panels of Fig. 9, are more tropospherically confined. The NH mode is weaker and the subpolar zonal wind anomalies are displaced poleward of their wintertime position. Results for the SH midwinter inactive season of JJA (not shown) are qualitatively similar to those for the summer inactive season.

In both hemispheres the temperature anomalies observed in association with the positive polarity of the annular modes (Fig. 9, lower panels) are similar to their active season counterparts with one notable exception: the prominent cold anomalies in the polar stratosphere are entirely absent. The equatorial tropopause (~100 hPa) remains anomalously warm, but the regression sections based on tropical tropopause temperature (not shown) are not as robust as their counterparts in Fig. 8 for the active seasons.

These results serve to confirm that the annular modes exist year-round, but that they are coupled with the high-latitude stratospheric circulation only during the active season in the respective hemispheres.

6. Zonally varying structures embedded in the annular modes

a. Lower-tropospheric temperature

TW98 argued that the AO is essentially an annular mode, whose zonally asymmetric thermal structure is induced by the land–sea distribution. A thermal signature virtually identical to the one they identified can be obtained by regressing monthly JFM NH surface air temperature (SAT) anomalies onto the standardized 1958–97 AO index (Fig. 10b). The positive polarity of the JFM AO is associated with positive SAT anomalies throughout high latitudes of Eurasia and much of North America, and negative anomalies over extreme eastern Canada, North Africa, and the Middle East. This zonally asymmetric pattern of SAT anomalies is evident throughout the year except during the NH summer months (not shown).

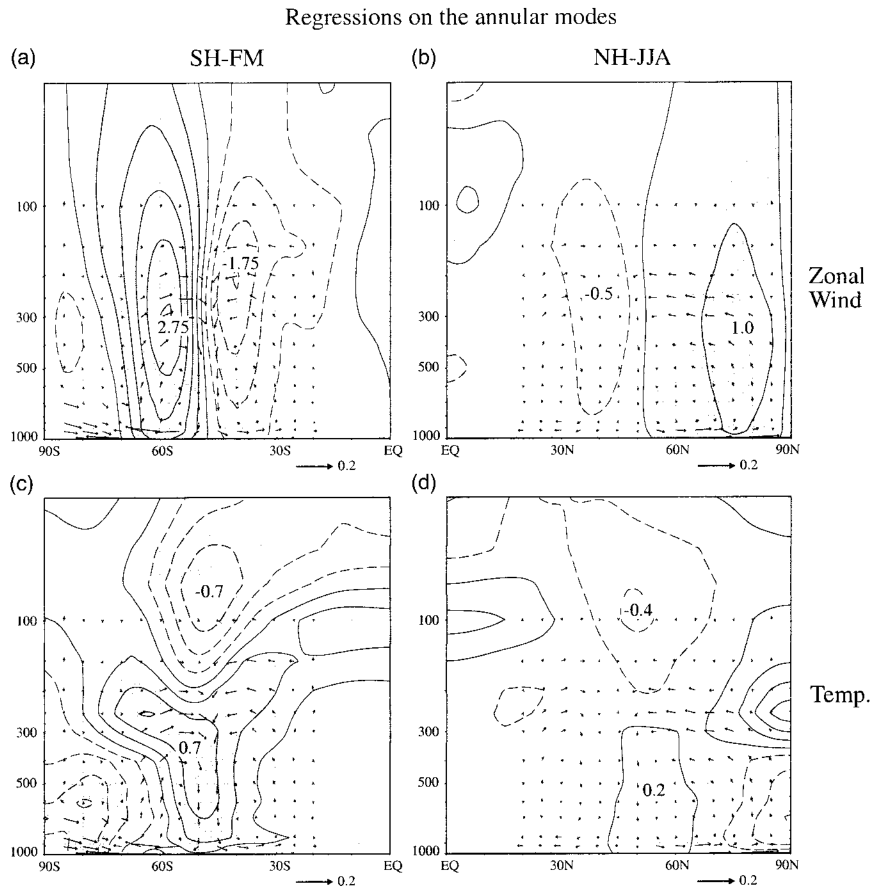

FIG. 9. As in Fig. 7 but for the inactive seasons Feb–Mar in the SH and Jun–Aug in the NH.

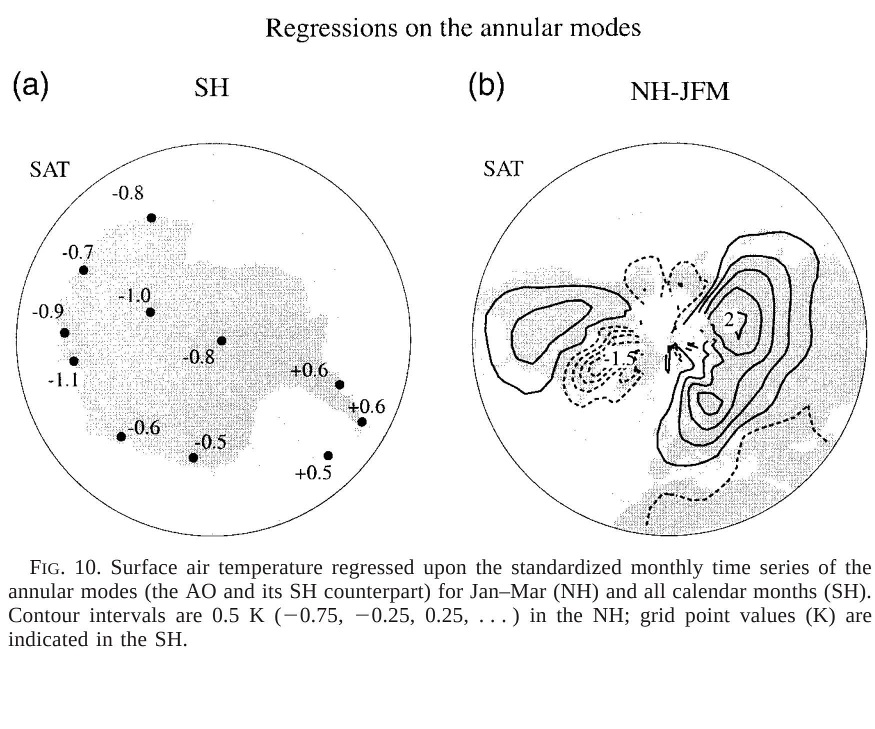

FIG. 10. Surface air temperature regressed upon the standardized monthly time series of the annular modes (the AO and its SH counterpart) for Jan–Mar (NH) and all calendar months (SH). Contour intervals are 0.5 K (−0.75, −0.25, 0.25, . . .) in the NH; grid point values (K) are indicated in the SH.

FIG. 11. (top) Vertically averaged (925–500 hPa) horizontal wind anomalies regressed upon the standardized AO index (vectors) and the vertically averaged (925–500 hPa) climatological mean temperature field (contours) for the active season Jan–Mar. (middle) Vertically averaged horizontal temperature advection by the zonal-mean zonal component of the flow in the top panel. (bottom) 500–1000-hPa thickness regressed upon the standardized Jan–Mar AO index. ← Contour intervals are 5 K (−27.5, −22.5, −17.5, . . .) for climatological mean temperature, 0.1 K day^{-1} (−0.15, −0.5, 0.5, . . .) for horizontal temperature advection, and 10 m (−15, −5, 5, . . .) for lower tropospheric thickness. Vectors are in units of m s^{-1}; scale at bottom of figure.

The patterns shown in Fig. 11 suggest that horizontal temperature advection plays a major role in maintaining these SAT anomalies. The top panel shows the vertically averaged (925–500 hPa) horizontal wind anomaly field regressed upon the standardized AO index for JFM, superposed upon the JFM climatological mean temperature field for the same layer. A similar map based on indices of the NAO is shown in Xie et al. (1999). Consistent with the zonal-mean zonal flow relationships documented in sections 3 and 5, the positive polarity of the AO is associated with westerly anomalies poleward of ~40°N and easterly anomalies to the south of that latitude. It is evident from the top panel of Fig. 11 that the zonal component of the flow over much of the NH high latitudes is directed across the climatological temperature gradient: downgradient on the eastern sides of the high-latitude continents and upgradient over the western sides.

The anomalous temperature advection induced by the zonal mean of the zonal component of the anomalous wind vectors $(-[u'](\partial/\partial x)\overline{T}$ where $[u']$ is the zonal mean of the anomalous zonal wind field and $\overline{T}$ the climatological-mean temperature field shown in the top panel) is shown in the middle panel of Fig. 11, expressed in units of K day^{-1}. Zonal-mean zonal flow anomalies associated with the high index polarity of the AO induce a pattern of temperature advection that resembles the pattern of SAT anomalies shown in Fig. 10: warm advection is found over Northern Europe, Siberia, and north-central North America, and cold advection is found over the northwest Atlantic and eastern Siberia. This pattern also resembles the structure of lower-tropospheric thickness anomalies obtained by regressing the 1000–500-hPa thickness field onto the standardized JFM AO index (Fig. 11 bottom). Regions of cold advection tend to coincide with negative thickness anomalies, and vice versa. The correspondence, though not perfect, is strong enough to support the notion that temperature advection by the zonal component of the anomalous flow plays an important role in establishing and maintaining the stationary wave pattern associated with the AO.

The data coverage over high latitudes of the SH is insufficient to support a comprehensive analysis of the anomalous SAT pattern associated with the annular mode. Rather than attempting such an analysis we show, in the left panel of Fig. 10, just the regression coefficients for grid points with data for 200 out of the maximum possible 480 months during the period 1958–97. The corresponding correlations at each grid point (not

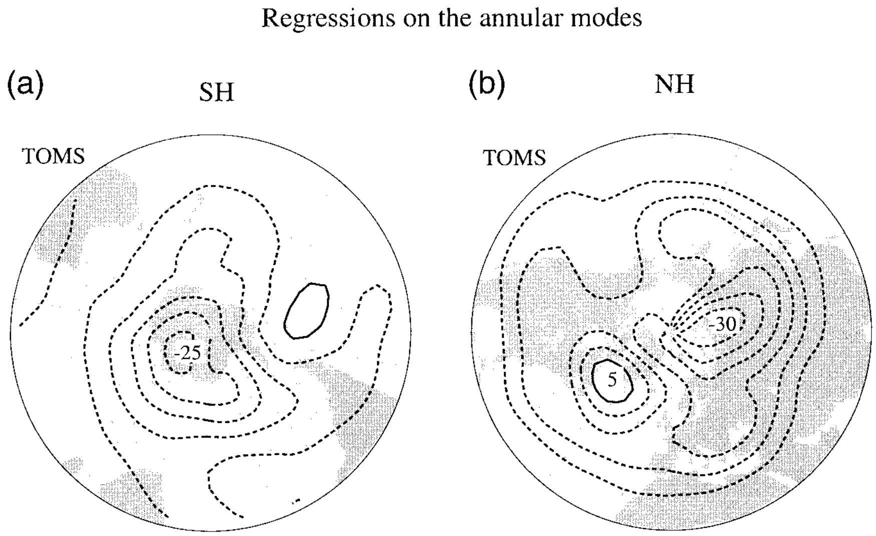

FIG. 12. Total column ozone regressed upon the standardized monthly time series of the annular modes (the AO and its SH counterpart) for the active season months of Mar (NH) and Nov (SH). Contour intervals are 5 Dobson units (−7.5, −2.5, 2.5, . . .).

shown) are all significant at the 99% level based on the *t* statistic. The positive polarity of the SH annular mode is associated with cold anomalies over most of Antarctica, consistent with its equivalent barotropic structure documented in Figs. 7 and 9. The one notable exception is the Antarctic peninsula, where the enhanced westerlies associated with the high index polarity (Fig. 1) increase the advection of relatively warm oceanic air over the cold land. This structure is evident throughout the year in the SAT field but there is no hint of it in the lower-tropospheric thickness field in the NCEP–NCAR reanalysis (not shown).

b. Total column ozone

The signature of the annular modes in total column ozone was investigated using TOMS data for the period of record of the *Nimbus-7* satellite (November 1978–April 1993), focusing on the active seasons when the annular modes amplify with height upward into the lower stratosphere. The NH analysis is restricted to March, the only active season month with sufficient sunlight over the polar cap region to provide a basis for measurements. Hence, the analysis is based on only 15 temporal samples (November 1978–92 in the SH; March 1979–93 in the NH). The strong correspondence between total ozone and tropopause pressure, which is available from the NCEP–NCAR reanalysis, enables us to verify the results on the basis of a much longer record including NH data for January and February as well as March. The patterns shown here were found to be highly reproducible in the proxy record. Corresponding relationships for the inactive season (not shown) are much weaker.

Figure 12 shows total column ozone regressed onto the standardized November SH index (left) and March NH index (right) of the respective annular modes. The NH pattern contains zonal asymmetries that tend to mirror the structure of thickness anomalies in the lower troposphere: a relative ozone maximum (suggestive of a depressed tropopause) is observed over the Labrador Sea where the lower troposphere is anomalously cold during the ''high index'' polarity of the AO, and a minimum is centered over Siberia where the lower troposphere is anomalously warm. Superposed upon these asymmetric features is a prevalence of negative anomalies in total column ozone over the entire region poleward of 40°N. March total column ozone over the region poleward of 40°N is correlated with the AO index at a level of −0.66: a one standard deviation change in the monthly AO index corresponds to a 12 Dobson unit change, equivalent to ~10% of the peak-to-peak amplitude of the annual march in total column ozone over this region and ~3% of the annual mean total column ozone. The positive polarity of the AO is also marked by increased ozone in the Tropics, indicative of a lowering of the tropopause, consistent with the zonal-mean temperature structures shown in section 5. The correlation coefficient between March total column ozone averaged 20°N–20°S and the AO index is +0.54.

The positive polarity of the SH annular mode is also associated with negative ozone anomalies over much of the high latitudes, but the correlations are not as strong as in the NH. This relationship is also evident in tropopause pressure (not shown). The zonally asymmetric feature near the southern tip of South America is not reproducible and may be a reflection of sampling variability.

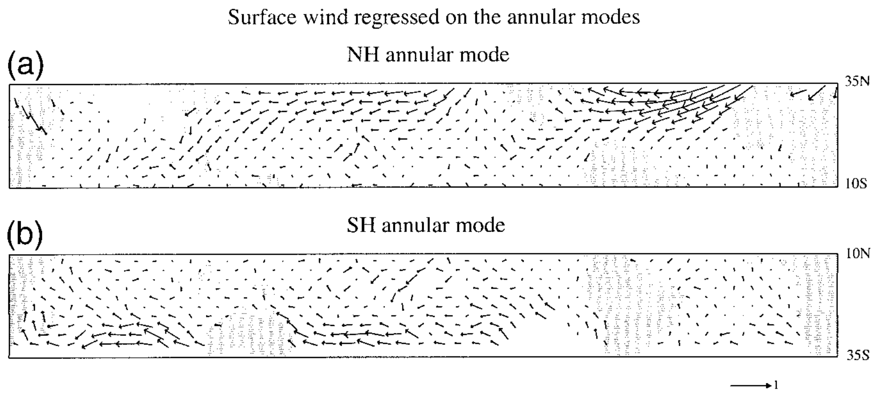

FIG. 13. Horizontal surface wind anomalies from the COADS (Table 1) regressed upon the year-round standardized monthly time series of the annular modes: (a) the AO and (b) its SH counterpart. Vectors are in units of m s^{-1}; scale at bottom of figure.

7. Discussion

The annular modes perturb the meridional profile of the westerlies in somewhat the same manner as envisioned by Namias (1950) in his description of the zonal ''index cycle.'' In the high index (positive polarity) state, the westerlies and the baroclinicity are enhanced at high latitudes and weakened near the core of the jet stream. The belt of poleward eddy fluxes is displaced poleward of its climatological mean position, together with the poleward limit of the Hadley cell and the entire Ferrell cell. Midlatitudes are anomalously warm, and the polar cap region is anomalously cold aloft. During the seasons when the lower-stratospheric polar vortex is susceptible to vigorous wave–mean flow interactions, the cold anomalies in the polar cap region intensify with height up to the 100-hPa level and the stratospheric polar vortex is anomalously strong. In the NH, total column ozone tends to be below normal, not only within the polar cap region, but also in the 40°–60° latitude belt, where the tropopause is raised in association with the anomalous warmth of the troposphere and the anticyclonic shear of the zonal flow at the tropopause level.

Embedded within the perturbed zonally symmetric flow is a distinctive pattern of tropospheric stationary wave perturbations. The high index polarity of the AO is characterized by anomalous warmth over most of North America and Eurasia poleward of 40°N at the earth's surface. The strongest anomalies are observed over Russia. An analogous but much smaller warm patch covers the Antarctic peninsula in association with the high index polarity of the SH annular mode.

The signature of the annular modes is not restricted to the extratropics. Their high index polarity is also characterized by a pattern of positive temperature anomalies observed near the equator at the 100-hPa level suggestive of a depression of the tropical tropopause. The high index polarity of the annular modes is also associated with easterly surface wind anomalies that extend deep into the subtropics. Figure 13, which shows regression maps based on the Comprehensive Ocean–Atmosphere Data Set (COADS) (Table 1), documents this relationship in further detail. In the high index state, the trade winds are strengthened in all ocean basins. Consistent with the SLP pattern shown in Fig. 1, the AO exhibits a particularly strong signature over the subtropical North Atlantic.

Consistent with more comprehensive momentum flux diagnostics based on both the observed SH annular mode (Yoden et al. 1987; Shiotani 1990; Karoly 1990; Kidson and Sinclair 1995; Hartmann and Lo 1998) and numerical simulations of the annular mode with zonally uniform lower boundary conditions (Robinson 1991, 1994, 1996; Yu and Hartmann 1993; Lee and Feldstein 1996; Feldstein and Lee 1996), and with realistic SH land–sea geometry (Kidson and Watterson 1999), it can be inferred from the sense of the mean meridional circulation in Figs. 7 and 9 that perturbations in the zonally averaged zonal wind above the planetary boundary layer in the SH annular mode must be maintained by anomalous eddy fluxes of zonal momentum. The same is evidently true of the AO. The rather strong correspondence between the rising and sinking branches of the mean meridional circulations and the anomalously cold and warm latitude belts in Figs. 7 and 9 suggests that the mean meridional circulations may be instrumental in maintaining the associated temperature anomalies.

Above the tropopause level, the mean meridional circulations in the NCEP–NCAR reanalysis do not exhibit a coherent pattern. However, the positive temperature anomalies at the tropical tropopause and the negative anomalies in the polar stratosphere that occur in association with the high index polarity of the annular modes are indicative of an overall weakening of the equator-to-pole wave driven, Lagrangian mean meridional circulation in the stratosphere.

We have presented circumstantial evidence in Fig. 11 to the effect that horizontal temperature advection by the zonal component of the flow in the lower troposphere plays an important role in setting up the stationary wave pattern associated with the AO. In a similar manner, it seems plausible that anomalously strong westerlies could maintain the above-normal surface air temperatures over the Antarctic Peninsula observed in association with the positive polarity of the SH annular mode. Whether the convergence of eddy heat fluxes by the baroclinic waves also contributes to the warmth of Eurasia during the positive polarity of the AO, as suggested by Rogers and Thompson (1995), remains to be seen. However, a preliminary analysis of J. W. Hurrell (1998, personal communication) indicates that the transient eddy fluxes act to damp rather than maintain the stationary wave pattern in the lower-tropospheric temperature field, consistent with their role in relation to blocking related anomalies (Mullen 1987) and to the climatological-mean stationary waves (Lau and Holopainen 1984). A quantitative assessment of the processes that give rise to the zonally varying features in the annular modes will require numerical experiments with a linearized, baroclinic stationary wave model. This approach has been used by Ting et al. (1996) to investigate the stationary wave response to the observed patterns of variability of the NH wintertime 500-hPa zonally averaged zonal flow. As documented in Wallace et al. (2000), the dominant mode of variability identified by Ting et al. (1996) on the basis of their numerical experiments closely resembles the AO.

The strong similarity between the meridional structures of the NH and SH annular modes despite the sharply contrasting land–sea distributions and stationary wave climatologies of the two hemispheres attests to the robustness of their many common features. Most notable among the distinctions between them is the seasonality: the AO is coupled with the NH stratospheric circulation throughout a 3–4-month-long midwinter season, whereas the SH mode is coupled with the stratospheric circulation only during a 6–8-week interval centered in November, well into the austral spring. These are the seasons in which wave–mean flow interactions in the lower stratosphere of the respective hemispheres are active and stratospheric temperatures over the polar cap regions are susceptible to episodic warmings. Baldwin and Dunkerton (1999) show that fluctuations in the AO during wintertime are inextricably linked to sudden warmings, which appear first near the 10-hPa level, and propagate downward into the lower stratosphere and troposphere on a timescale of weeks. Fluctuations in the SH annular mode during November are associated with year-to-year differences in the timing of the spring warmings that signal the breakdown of the midwinter polar vortex.

Because of the shorter duration of the active season in the SH, which spans only one active calendar month per year (compared to three in the NH), statistics relating to the SH annular mode are subject to larger sampling variability. The uncertainties are compounded by concerns about the adequacy of the NCEP–NCAR reanalysis in high latitudes of the SH. Nonetheless, the three-dimensional structure of the SH annular mode appears to be almost as spatially coherent and no less dynamically consistent than that of the AO.

The pervasiveness of the annular modes in simple two-layer models (Robinson 1991, 1994, 1996; Lee and Feldstein 1996), multilayer numerical simulations with zonally symmetric boundary conditions (James and James 1992; Yu and Hartmann 1993; Feldstein and Lee 1996), and general circulation models with realistic land–sea geometry (Fyfe et al. 1999; von Storch 1999; Kidson and Watterson 1999; Shindell et al. 1999; Volodin and Galin 1998a, 1998b) attests to the simplicity and robustness of the dynamical selection process to which they owe their existence. We will defer speculation on what that process might be until the final section of Part II (Thompson et al. 2000), after we show that the climatic trends observed over the past 30 yr during the stratosphere's active season bear a remarkable similarity to the structure of the annular modes.

Acknowledgments. Please see Part II.

REFERENCES

Baldwin, M. P., and T. J. Dunkerton, 1999: Propagation of the Arctic Oscillation from the stratosphere to the troposphere. *J. Geophys. Res.,* **104,** 30 937–30 946.

——, X. Cheng, and T. J. Dunkerton, 1994: Observed correlations between winter-mean tropospheric and stratospheric circulation anomalies. *Geophys. Res. Lett.,* **21,** 1141–1144.

Charney, J. G., and P. G. Drazin, 1961: Propagation of planetary-scale disturbances from the lower into the upper atmosphere. *J. Geophys. Res.,* **66,** 83–109.

Cheng, X., and T. J. Dunkerton, 1995: Orthogonal rotation of spatial patterns derived from singular value decomposition analysis. *J. Climate,* **8,** 2631–2643.

Feldstein, S., and S. Lee, 1996: Mechanisms of zonal index variability in an aquaplanet GCM. *J. Atmos. Sci.,* **53,** 3541–3555.

Fyfe, J. C., G. J. Boer, and G. M. Flato, 1999: The Arctic and Antarctic Oscillations and their projected changes under global warming. *Geophys. Res. Lett.,* **26,** 1601–1604.

Gong, D., and S. Wang, 1999: Definition of Antarctic Oscillation index. *Geophys. Res. Lett.,* **26,** 459–462.

Hartmann, D. L., and F. Lo, 1998: Wave-driven zonal flow vacillation in the Southern Hemisphere. *J. Atmos. Sci.,* **55,** 1303–1315.

James, I. N., and P. M. James, 1992: Spatial structure of ultra-low frequency variability of the flow in a simple atmospheric circulation model. *Quart J. Roy. Meteor. Soc.,* **118,** 1211–1233.

Jones, P. D., 1994: Hemispheric surface air temperature variations: A reanalysis and update to 1993. *J. Climate,* **7,** 1794–1802.

Kalnay, E. M., and Coauthors, 1996: The NCEP/NCAR Reanalysis Project. *Bull. Amer. Meteor. Soc.,* **77,** 437–471.

Karoly, D. J., 1990: The role of transient eddies in low-frequency zonal variations of the Southern Hemisphere circulation. *Tellus,* **42A,** 41–50.

Kidson, J. W., 1988a: Indices of the Southern Hemisphere zonal wind. *J. Climate,* **1,** 183–194.

——, 1988b: Interannual variations in the Southern Hemisphere circulation. *J. Climate,* **1,** 1177–1198.

——, and M. R. Sinclair, 1995: The influence of persistent anomalies on Southern Hemisphere storm tracks. *J. Climate,* **8,** 1938–1950.

——, and I. G. Watterson, 1999: The structure and predictability of the ''high-latitude mode'' in the CSIRO9 general circulation model. *J. Atmos. Sci.,* **56,** 3859–3873.

Kitoh, A., H. Koide, K. Kodera, S. Yukimoto, and A. Noda, 1996: Interannual variability in the stratospheric-tropospheric circulation in a coupled ocean-atmosphere GCM. *Geophys. Res. Lett.*, **23,** 543–546.

Kodera, K., M. Chiba, H. Koide, A. Kitoh, and Y. Nikaidou, 1996: Interannual variability of the winter stratosphere and troposphere in the Northern Hemisphere. *J. Meteor. Soc. Japan,* **74,** 365–382.

Kutzbach, J. E., 1970: Large-scale features of monthly mean Northern Hemisphere anomaly maps of sea-level pressure. *Mon. Wea. Rev.,* **98,** 708–716.

Lau, N.-C., and E. O. Holopainen, 1984: Transient eddy forcing of the time-mean flow as identified by geopotential tendencies. *J. Atmos. Sci.,* **41,** 313–328.

Lee, S., and S. Feldstein, 1996: Mechanism of zonal index evolution in a two-layer model. *J. Atmos. Sci.,* **53,** 2232–2246.

Mullen, S. L., 1987: Transient eddy forcing of blocking flow. *J. Atmos. Sci.,* **44,** 3–22.

Namias, J., 1950: The index cycle and its role in the general circulation. *J. Meteor.,* **7,** 130–139.

National Aeronautics and Space Administration, 1978: *The Nimbus 7 Users' Guide.* C. R. Madrid, Ed., Goddard Space Flight Center.

North, G. R., T. L. Bell, R. F. Cahalan, and F. J. Moeng, 1982: Sampling errors in the estimation of empirical orthogonal functions. *Mon. Wea. Rev.,* **110,** 699–706.

Parker, D. E., C. K. Folland, and M. Jackson, 1995: Marine surface temperature: Observed variations and data requirement. *Climatic Change,* **31,** 559–600.

Perlwitz, J., and H.-F. Graf, 1995: The statistical connection between tropospheric and stratospheric circulation of the Northern Hemisphere in winter. *J. Climate,* **8,** 2281–2295.

Randel, W. J., and F. Wu, 1999: Cooling of the Arctic and Antarctic polar stratospheres due to ozone depletion. *J. Climate,* **12,** 1467–1479.

Robinson, W. A., 1991: The dynamics of the zonal index in a simple model of the atmosphere. *Tellus,* **43A,** 295–305.

——, 1994: Eddy feedbacks on the zonal index and eddy-zonal flow interactions induced by zonal flow transience. *J. Atmos. Sci.,* **51,** 2553–2562.

——, 1996: Does eddy feedback sustain variability in the zonal index? *J. Atmos. Sci.,* **53,** 3556–3569.

Rogers, J. C., and H. van Loon, 1982: Spatial variability of sea level pressure and 500-mb height anomalies over the Southern Hemisphere. *Mon. Wea. Rev.,* **110,** 1375–1392.

——, and E.-M. Thompson, 1995: Atlantic Arctic cyclones and the mild Siberian winters of the 1980s. *Geophys. Res. Lett.,* **22,** 799–802.

Shindell, D. T., R. L. Miller, G. Schmidt, and L. Pandolfo, 1999: Simulation of recent northern winter climate trends by greenhouse-gas forcing. *Nature,* **399,** 452–455.

Shiotani, M., 1990: Low-frequency variations of the zonal mean state of the Southern Hemisphere troposphere. *J. Meteor. Soc. Japan,* **68,** 461–471.

Spencer, R. W., and J. R. Christy, 1993: Precision lower stratospheric temperature monitoring with the MSU: Technique, validation, and results 1979–1991. *J. Climate,* **6,** 1194–1204.

Szeredi, I., and D. J. Karoly, 1987: Horizontal structure of monthly fluctuations of the Southern Hemisphere troposphere from station data. *Austr. Meteor. Mag.,* **35,** 119–129.

Thompson, D. W. J, and J. M. Wallace, 1998: The Arctic Oscillation signature in the wintertime geopotential height and temperature fields. *Geophys. Res. Lett.,* **25,** 1297–1300.

——, ——, and G. C. Hegerl, 2000: Annular modes in the extratropical circulation. Part II: Trends. *J. Climate,* **13,** 1018–1036.

Ting, M., M. P. Hoerling, T. Xu, and A. Kumar, 1996: Northern Hemisphere teleconnection patterns during extreme phases of the zonal-mean circulation. *J. Climate,* **9,** 2614–2633.

Trenberth, K. E., and D. A. Paolino, 1980: The Northern Hemisphere sea level pressure data set: Trends, errors and discontinuities. *Mon. Wea. Rev.,* **108,** 855–872.

——, and ——, 1981: Characteristic patterns of variability of sea level pressure in the Northern Hemisphere. *Mon. Wea. Rev.,* **109,** 1169–1189.

Volodin, E. M., and V. Ya. Galin, 1998a: Sensitivity of midlatitude Northern Hemisphere winter circulation to ozone depletion in the lower stratosphere. *Russ. Meteor. Hydrol.,* **8,** 23–32.

——, and ——, 1998b: Investigation of the first mode of low-frequency variability of winter atmospheric circulation in the midlatitudes of the Northern Hemisphere. *Russ. Meteor. Hydrol.,* **9,** 26–40.

von Storch, J.-S., 1999: The reddest atmospheric modes and the forcings of the spectra of these modes. *J. Atmos. Sci.,* **56,** 1614–1626.

Wallace, J. M., and D. S. Gutzler, 1981: Teleconnections in the geopotential height field during the Northern Hemisphere winter. *Mon. Wea. Rev.,* **109,** 784–812.

——, D. W. J. Thompson, and Z. Fang, 2000: Comments on ''Northern Hemisphere teleconnection patterns during extreme phases of the zonal-mean circulation.'' *J. Climate,* **13,** 1037–1039.

Woodruff, S. D., R. J. Slutz, R. L. Jenne, and P. M. Steurer, 1987: A comprehensive ocean–atmosphere data set. *Bull. Amer. Meteor. Soc.,* **68,** 1239–1250.

——, S. J. Lubker, K. Wolter, S. J. Worley, and J. D. Elms, 1993: Comprehensive Ocean-Atmosphere Data Set (COADS) Release 1a: 1980–92. *Earth System Monitor,* **4** (1), 1–8.

Xie, S.-P., H. Noguchi, and S. Matsumura, 1999: A hemispheric-scale quasi-decadal oscillation and its signature in Northern Japan. *J. Meteor. Soc. Japan,* **77,** 573–582.

Yoden, S., M. Shiotani, and I. Hirota, 1987: Multiple planetary flow regimes in the Southern Hemisphere. *J. Meteor. Soc. Japan,* **65,** 571–586.

Yu, J.-Y., and D. L. Hartmann, 1993: Zonal flow vacillation and eddy forcing in a simple GCM of the atmosphere. *J. Atmos. Sci.,* **50,** 3244–3259.